Geophysical Journal International

Geophys. J. Int. (2011) **186,** 32–44 doi: 10.1111/j.1365-246X.2011.05035.x

A major step in the continental Moho and its geodynamic consequences: the Taranaki–Ruapehu line, New Zealand

M. L. Salmon,[1,2] T. A. Stern[2] and M. K. Savage[2]

[1] *RSES, Australian National University, Canberra, Australia*

[2] *Institute of Geophysics, Victoria University of Wellington, New Zealand. E-mail: tim.stern@vuw.ac.nz*

Accepted 2011 April 3. Received 2011 March 1; in original form 2010 November 11

SUMMARY

Receiver function analysis reveals a 7 km step-like change in crustal thickness across the Taranaki–Ruapehu Line (TR-line) of North Island, New Zealand. The TR-line runs east–west between the active andesite volcanoes of Mt Taranaki and Ruapehu and marks the southernmost extent of subduction zone volcanism in New Zealand. North of the TR-line receiver functions show a strong and sharp *P*-to-*S* (*Ps*) conversion at 25 ± 1.5 km depth, which is interpreted as a shallow Moho. At the TR-line the Moho *Ps* conversion deepens across a step to ∼32 km depth and weakens. Further south the Moho deepens to >35 km. Most of the 7 km step-change in crustal thickness occurs over a lateral distance of ∼8 km, yet there is little surface or topographic manifestation of the line. Given Fresnel zone considerations, the dip of the Moho offset could vary between 90° and 45°. Gravity, seismic attenuation and electrical data all show that the TR-line is not only a step in crustal thickness but also a profound lithospheric boundary as mantle properties, such as attenuation (Q_p^{-1}), implied density, and electrical resistivity change abruptly across the line. An east–west oriented cluster of earthquakes with hypocentral depths of 20–40 km is centred on the Moho step. We propose that the Moho step, the earthquakes and the rapid change in mantle properties across the TR boundary are causally related. Processes that could be responsible for the phenomena described here include the rapid removal of mantle lithosphere and lower crust to the north of the TR-line.

Key words: Body waves; Intra-plate processes; Neotectonics; Rheology: crust and lithosphere.

1 INTRODUCTION

Behind active continental margins tectonic processes can vary from active extension to compression in both space and time (Dickinson 2003). Deciphering the transition from one type of regime to another is often difficult because of tectonic overprinting. In central North Island, New Zealand, where back-arc spreading is mainly Pliocene in age, there are clear geophysical signals of where such a transition occurs across the Taranaki–Ruapehu Line (TR-line; Fig. 1). Volcanism in the back-arc region of North Island has migrated southward over the past 27 Myr (Hayward *et al*. 2001) and the TR-line marks the southern extent of subduction zone volcanism in New Zealand. There is, however, a clear distinction between the low-K andesites that define the migrating plate boundary beneath North Island starting in the Miocene, and the high-K andesites/basalts of western North Island that are all Pliocene in age and do not appear to align themselves with the modern plate boundary (Hatherton 1969; Stern *et al.* 2006). For example, although Mt Ruapehu is classically related to a subjacent Wadati-Benioff zone at a depth of ∼100 km, Mt Taranaki is not (Fig. 1). The Wadati-Benioff zone is at a depth of ∼180 km beneath Mt Taranaki (Adams & Ware 1977; Reyners *et al.* 2006) and the geochemistry of its lavas is at variance with classical subduction zone andesites (Hatherton 1969; Price *et al.* 1999).

First recognition of an important deep-reaching, east–west boundary in the New Zealand lithosphere goes back to work on attenuation of earthquake waves in the mantle (Mooney 1970). North and south of this east–west boundary, there was attenuation and transmission of high frequency earthquake waves, respectively. The initial position of what was then termed the attenuating-transmitting boundary was ∼20 km south of the TR-line, but later work shows them to be virtually coincident (Salmon *et al.* 2005; Stern *et al.* 2006; Eberhart-Phillips *et al.* 2008). By the mid 1980s crustal structure exploration showed a crustal thickness of ∼25 km over much of NW North Island (Stern *et al.* 1987), yet 40 km to the south of the TR-line, in the Wanganui Basin (Fig. 2), crustal thickness is ∼42 km (Holt & Stern 1994). More recent work highlighted that the mantle lid is largely absent or heavily thinned north of the TR-line based on P_n and S_n wave speeds and receiver functions (Horspool *et al.* 2006; Seward *et al.* 2008, 2009). A change in mantle anisotropy between highly coherent, north–south oriented fast polarisations south of the line and incoherent or absent anisotropy north of the line (Audoine *et al.* 2004; Greve *et al.* 2008) can also be interpreted to be caused

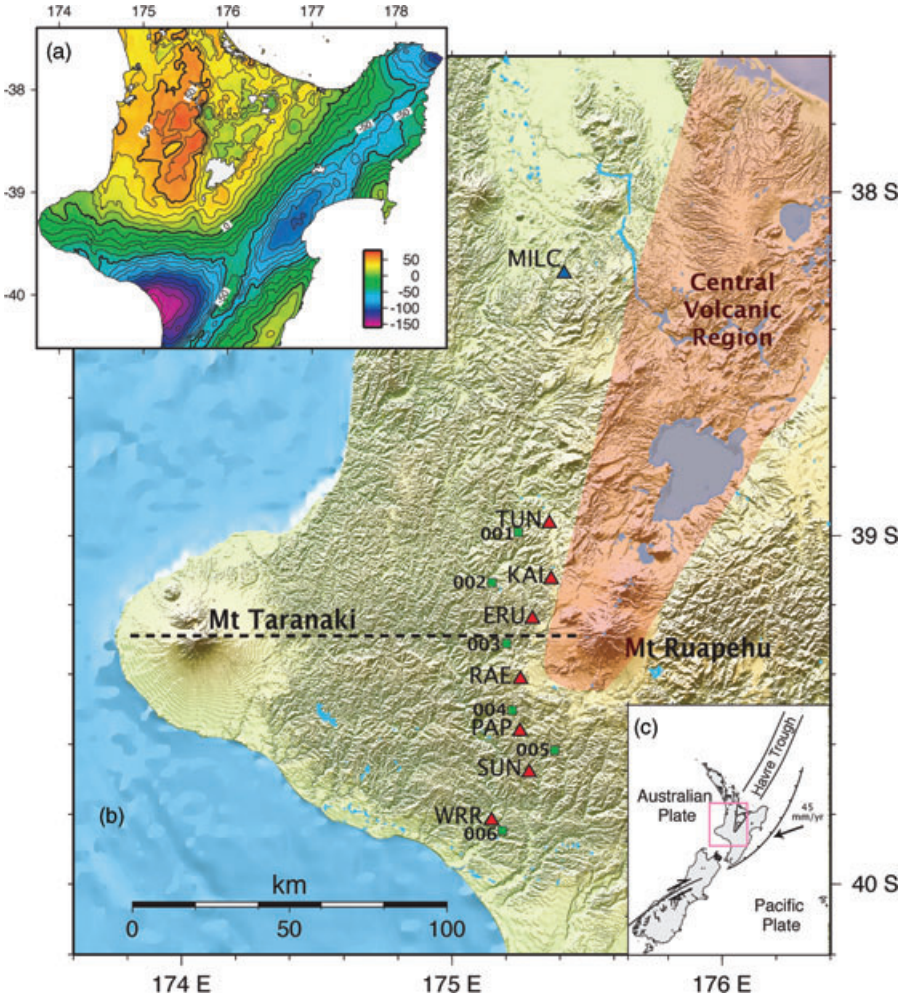

Figure 1. (a) Isostatic gravity map for the North Island, New Zealand. Units = mGal. (b) Location map superimposed on a digital elevation map for the TRAP array along a north–south road between the active andesite volcanoes of Mts Taranaki and Ruapehu. The TR-line referred to the text runs between these two volcanoes and in shown as a dashed line. Red triangles represent the seven locations of seismographs from which the analysis is based. The one blue triangle represents the MILC seismic station from a previous receiver function experiment referred to in the text. Green squares are sites of MT stations shown in Fig. 8. (c) Plate tectonic location map for New Zealand showing the position of the study area, the plate boundary between the Australian and Pacific plates and the vector of velocity for the Pacific Plate with respect to a fixed Australian Plate. The Pacific Plate subducts beneath the Australian Plate.

by sheared thick lithosphere to the south and absence of such lithosphere to the north. What was not clear was exactly where and how the north to south transition in crustal and lithospheric thickness took place.

A steep gravity gradient whose maximum corresponds closely with the TR-line (Fig. 1), was interpreted as an isostatically compensated step in the Moho of ∼10 km (Stern *et al.* 1987). Steps in the continental Moho are rare, imply high deviatoric stresses and require a special explanation (McBride 1994). Where they have been documented they are often linked to strike slip zones (Doll *et al.* 1996; Zhu & Kanamori 2000; Wilson *et al.* 2004). No strike-slip zone is associated with the TR-line, nor indeed is any other type of faulting (New Zealand Geological Survey 1972). All mapped faults in the vicinity run nearly perpendicular to it (Fig. 2). Thus the nature and origin of the crust and mantle offset at or adjacent to the TR-line appears to be an unusual phenomenon that could hold clues to the origin of back-arc structures in general. This study is, therefore, focussed on mapping the Moho boundary with receiver functions and exploring reasons for the sharp change in Moho depth beneath the TR-line.

2 RECEIVER FUNCTION METHOD AND DATA

2.1 Receiver function technique

The receiver function technique uses the mode conversions in the coda of near vertically travelling body waves from distant earthquakes to gain information about the earth below the seismograph (Langston 1979; Owens & Zandt 1985; Wilson *et al.* 2004). Receiver functions are particularly useful for imaging sharp offsets in converting boundaries because the ray-paths of the seismic waves used are near vertical. If the Taranaki-Ruapehu Line is manifest as a rapid change in crustal thickness, a receiver function profile across the line should therefore provide a test of the magnitude of the offset and its location.

2.2 Data collection and analysis

The Taranaki-Ruapehu Attenuation Project (TRAP) array (Fig. 2) was initially set out to define attenuation in the upper mantle, and

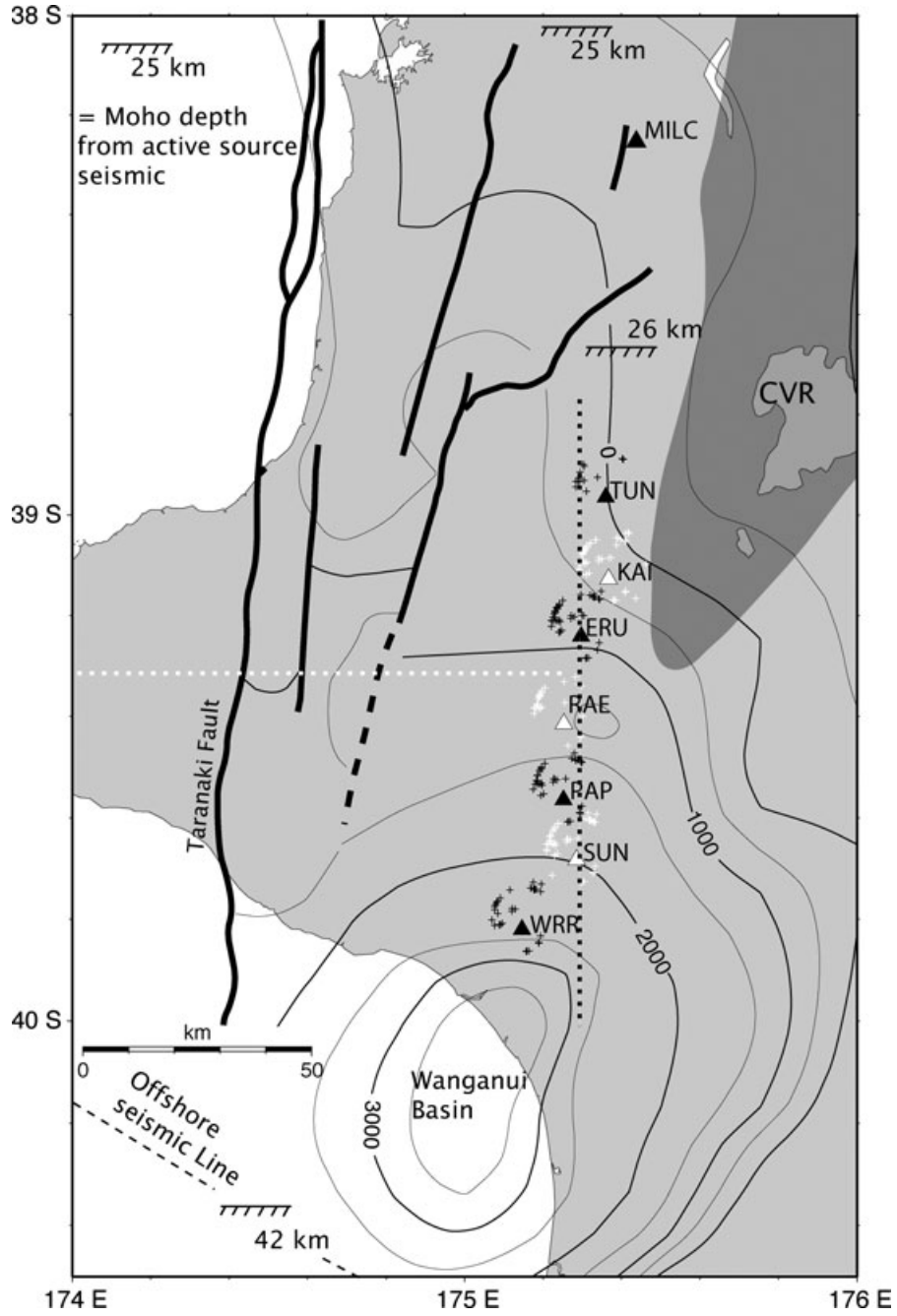

Figure 2. Station locations and 30-km depth piercing points. Station locations are indicated by the black or white triangles. Estimated piercing points for each station are shown as black or white crosses. Colours are alternated according to station so that piercing points for each station can be differentiated from each other. Depth contours of the Wanganui basin sediments are shown as thin lines (Anderton 1981). The dark grey shaded area indicates the extent of the Central Volcanic Region. Horizontal bars underlain by barbs are positions where Moho depths (given in km) have been determined with active source seismic methods. Onshore positions from Stratford & Stern (2006). Offshore from depth converted seismic reflection data (Holt & Stern 1994). The black dotted line shows the position of the transect in Fig. 6 and the white dotted line shows the position of the TR-line.

those results are reported elsewhere (Salmon 2008). All stations were equipped with L4C-3D 1 Hz seismometers and Reftek data loggers with a sampling rate of 100 Hz.

2.2.1 Earthquake selection

The National Earthquake Information Centre global catalogue provided a list of earthquakes with magnitudes $\geq$6.0 within an epicentral distance range of 10–110 degrees from the array. Although receiver functions are usually carried out on teleseismic events (epicentral distances $\geq 30^{\circ}$), regional events between 10° and 30° were also included to increase the azimuthal coverage. Instruments were deployed for up to 10 months. Over this time 79 earthquakes fitted the above criteria, 12 regional events and 67 teleseismic events. Most of the events originate in the region of the Banda Sea and Papua to the north west of New Zealand, providing good azimuthal coverage in this quadrant (Fig. 3b).

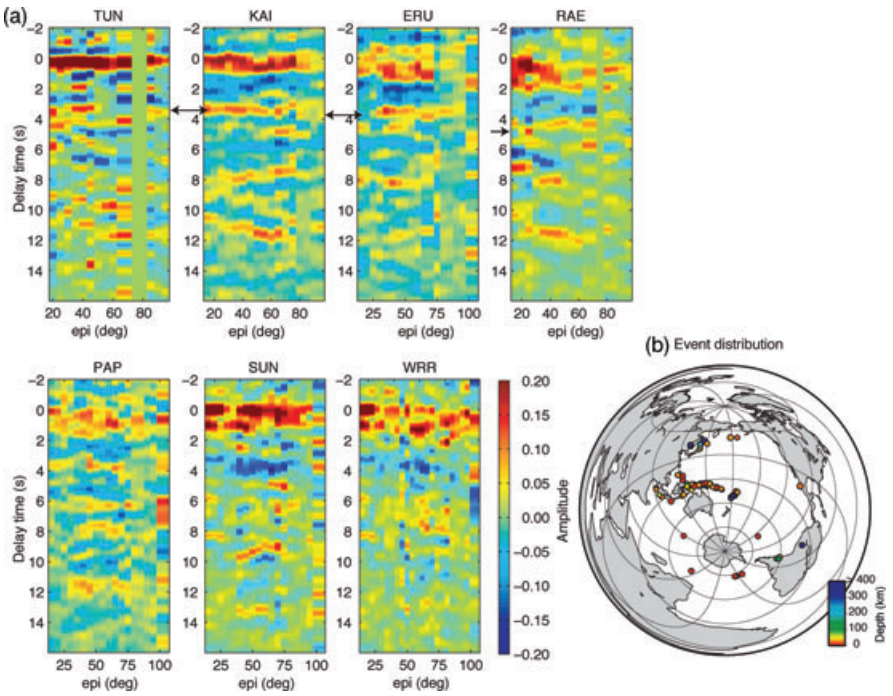

Figure 3. Receiver function results. (a) Receiver functions for each station stacked by epicentral distance. See text for parameters. Orange colours indicate positive phases, which indicate an increase in velocity with depth. Double headed arrows indicate Moho conversions for stations TUN KAI, ERU and RAE. (b) Location and depth of events used for the receiver functions.

Conversely there were few earthquakes recorded that originate east or south of New Zealand, giving poor azimuthal coverage in all other directions. Regional events that originate from the Tonga-Kermadec region increase the azimuthal coverage to the northeast. Events to the south and northeast are mostly $\geq 80^{\circ}$ away except for the Tonga-Kermadec events. Distant earthquakes will tend to have a lower signal-to-noise ratio (especially at higher frequencies) and will produce lower quality receiver functions. The number of events used at each station varied from 59 (station KAI) to just 15 (station TUN) depending on the deployment time for the station.

2.2.2 Data preparation and the receiver function method

Stations of the array were located on sediments of the Wanganui basin (Fig. 2). Several decades of oil exploration in the region allow an assessment of sediment depths below each station to be made. We constructed basement contour maps using drill hole data and seismic reflection lines (St John 1964; Watson & Allen 1964; Gerrard 1971; Anderton 1981; Fig. 2). Seismic refraction data in the area give *P*-wave velocities of 3.4 km s^{-1} for Miocene sediments and 5.3–5.5 km s^{-1} for the Mesozoic greywacke basement (Watson & Allen 1964). Sediment thickness increases from about 300 m in the north to >2 km at the southern end of the study area (Anderton 1981). We use these sediment thickness estimates to make corrections for the Moho conversion depths, as discussed in a following section.

Data were rotated into the LQT reference frame, an orthogonal reference frame where L is in the direction of the incident *P* wave (Vinnik 1977), using NEIC catalogue event locations, the AK135 global velocity model and assuming a low velocity surface layer with $Vp = 3.4$ km s^{-1}. The LQT frame suppresses the initial *P*-wave amplitude, so that all amplitudes observed are expected to be caused by mode conversions from structures beneath the surface. While it is more common for broad-band instruments to be used for receiver function studies, teleseismic events were recorded in this study with signal-to-noise ratios greater than 2 out to frequencies greater than 3 Hz. Such high frequency data can be problematic for both the spectral division and time domain deconvolution methods of calculating receiver functions. We have therefore used the multiple-taper correlation (MTC) method (Park & Levin 2000). MTC receiver functions are calculated using an 80 s time window for both pre-event noise and signal. Noise windows end ∼5 s before the predicted *P*-wave arrival and signal windows begin immediately after the noise window.

Frequency domain receiver functions are low-pass filtered using a cosine-squared filter with a corner frequency of 1.5 Hz. Frequency domain receiver functions for individual events are sorted into stacking bins for epicentral distance. Overlapping bins of 10° width are used so that each event contributes to two adjacent bins. The inverse-variances of the individual receiver functions are used as weights for stacking so that frequencies with a low coherence between the vertical and horizontal components will influence the stacked receiver function less than those that are strongly coherent (Park & Levin 2000).

Time domain receiver functions for the stacked spectra are calculated using an inverse Fourier transform and are normalised to preserve amplitudes using the normalisation factor $2f_N/f_c$ where f_N is the Nyquist frequency and f_c the corner frequency. There are no formal uncertainties for receiver functions in the time domain.

3 RECEIVER FUNCTION OBSERVATIONS

Receiver function results can be split into northern and southern groups, each with distinct characteristics (Fig. 3a). Positive amplitudes (red) indicate higher velocity below a boundary than above, and negative amplitudes indicate decreasing velocities with depth.

Because of the poor backazimuthal coverage, we do not discuss transverse receiver functions or the backazimuthal variation here. Salmon (2008) includes more detailed discussions of these aspects.

3.1.1 Northern station group

A distinct positive phase is observed near 0 s on the northern stations TUN and KAI, even though the direct arrival should be eliminated in the LQT reference frame (Fig. 3a). These arrivals occur somewhat after 0 s and are interpreted as conversions from shallow sediments directly under the stations. A positive peak is observed at 3.2, 3.3 and 3.4 s at stations TUN, KAI and ERU, respectively (Fig. 3a). Delay times for this peak increase southward with increasing sediment thickness.

TUN is the northern most station in the TRAP array and had the shortest deployment time. This station only recorded 15 events that could be used for receiver function analysis, thus limiting the backazimuth range and the number of events in each stacking bin. Receiver functions for this station show a strong positive peak with a small time delay (∼0.3 s) followed by a negative peak at 1.4 s (Fig. 3a). There is another positive peak at 3.2 s, which can be seen between 30° and 50° in epicentral distance.

Station KAI recorded 59 events that could be used in receiver function analysis (Fig. 3a). This station had the best azimuthal coverage of all the TRAP stations. As with station TUN, the first positive peak on the receiver functions is slightly offset from zero (0.1 s). This peak is followed by a negative peak (trough) that shifts from 2.2 s at an epicentral distance of 15° to 1.5 s at epicentral distances ≥60°. A positive peak is observed at 3.3 s, which is interpreted to be the Moho conversion at a depth ∼25 km (see later analysis). Two additional positive peaks can be seen, one between 7 and 8 s and another at between 11 and 12 s. The first of these two peaks has decreasing delay times with increasing epicentral distance, consistent with it being a *Ps* conversion from within the mantle. The delay time for the 11–12 s peak increases with increasing epicentral distance. This is consistent with the move out expected for a multiple (Ammon *et al.* 1990; i.e. a phase that is reflected from the surface and from a deeper layer). There is also a trough observed at ∼5.8 s.

Station ERU recorded 52 teleseismic events. The receiver functions are characterised by a band of positive energy out to 1.6 s followed by a band of negative energy out to 3.2 s (Fig. 3a). Both of these bands have a double peak. Positive peaks are observed at 3.4 and at ∼8 s and a trough is observed at 5.3 s. The 8 s peak is only a weak feature. Additional receiver functions are available for several stations to the north of this study (Bannister *et al.* 2007), of which station MILC is in line with the stations of this study ∼80 km north of TUN (Fig. 2). A Moho conversion at MILC is observed at a delay time of 3.2 s, which is close to those at TUN, ERU and KAI.

3.1.2 Southern station group

Receiver functions for the southern sites are characterised by longer period signals than those of the northern stations. RAE only recorded 28 events that could be used for receiver function analysis, since one of the horizontal components was malfunctioning for 5 months. Receiver functions show a similar pattern to those of station ERU. Radial receiver functions have a double peaked region of positive energy out to delay times of 2.1 s followed by a similar double peaked negative out to 4 s (Fig. 3a).

Receiver functions for the southern sites also have a negative peak between 6 and 7 s. This peak is largest for smaller epicentral distances and has a delay time that increases with epicentral distance, indicating that it is a multiple.

Station PAP recorded 45 teleseismic events. Receiver functions have a broad double peaked region of positive energy out to delay times of 2 s (Fig. 3a), similar to both stations ERU and RAE. It is followed by a broad region of negative peaks out to ∼6 s. Unlike the stations to the north, a positive peak in the 3–4 s delay time range is not coherent in the epicentral distance binned receiver functions. There are also weak positive peaks at ∼8 and ∼12 s.

Stations SUN and WRR are at the southern end of the TRAP line and recorded 55 and 35 teleseismic events respectively. Peaks on the radial components are difficult to trace over epicentral distance (Fig. 3a). Instead a region of dominantly positive energy out to ∼3 s followed by a band of dominantly negative energy out to ∼6 s is observed. Three peaks that can be traced over adjacent stacking bins for station SUN are a negative arrival at 5.6 s and two positives at ∼8 and ∼13 s.

4 INTERPRETATION

4.1 Piercing points

Although receiver functions use events with ray paths that have a near vertical incidence angle, there is a horizontal offset between where the ray pierces a boundary and the station. This offset distance is dependent on the ray parameter, p, the depth of the boundary (z), and the wave speed, c, between the boundary of interest and the receiver. The location where a ray path pierces a boundary (the piercing point) can be estimated using Snell's law. Moho piercing points have been estimated for each station assuming a 30 km thick crust, a V_s of 3.54 km s^{-1} and horizontal slowness parameters estimated from the AK135 travel time curves (Kennett *et al.* 1995; Fig. 2). Piercing point offsets for *Ps* conversions at 30 km depth range from 4.3 to 14.6 km. The lateral distance from the station sampled by the first surface *P* wave multiple that converts to an *S* wave (*PpPs*) can also be estimated using a *Vp* of 6.1 km s^{-1} and a boundary depth of 30 km, the distance the *PpPs* multiple samples is up to 65 km from the receiver. If structure varies laterally on this scale, multiples would be degraded and possibly absent.

Another consideration in lateral resolution is the radius of the Fresnel zone. Using a plane wave approximation (Sheriff & Geldart 1995) and assuming an *S*-wave velocity of 3.54 km s^{-1} [average crustal *S*-wave velocity for the New Zealand Standard velocity model (Sheriff & Geldart 1995)] and a frequency of 1.5 Hz, the Fresnel zone radius is ∼8 km for a depth of 30 km. Or in other words at a depth of 30 km any structure on the Moho will appear to be smeared laterally over a distance of 8 km.

4.1.1 Moho arrivals

The New Zealand standard (NZST) velocity model (Maunder 2002) gives an average crustal *Vp* of 6.1 km s^{-1} and *Vs* of 3.54 km s^{-1}. Using these velocities *Ps* conversions from the Moho would be expected at delay times (t_{Ps}) between 2.5 and 5.0 s for depths (H) between 20 and 40 km based on the following equation (Gurrola *et al.* 1994):

$$H = \frac{t_{Ps}}{\sqrt{1/Vp^2 - p^2} - \sqrt{1/Vp^2 - p^2}}, \quad (1)$$

where *Vs* and *Vp* are the *P*- and *S*-wave speeds in the crust, and p is the ray parameter, or horizontal slowness (Shearer 1999).

Along the array delay times for the Moho conversions (t_{Ps}) generally increase from north to south.

At RAE the Moho conversion arrives at 4.3 s (Fig. 3a), 0.9 s later than the station immediately to the north (ERU) and 1 s later than MILC 100 km to the north (Fig. 4). A 1 s change in delay time would require a 10 km change in crustal thickness or a 10–15 per cent increase in *Vp*/*Vs*. However receiver functions for this station sample the same basement terrane as the stations immediately to the north, there are no large-scale faults in the vicinity (Fig. 2) and (Reyners *et al.* 2006) show no significant increase in *Vp*/*Vs* ratio in this region. A change in crustal thickness is therefore proposed as the origin of the high delay-time at station RAE. This station is close to a steep gradient in the isostatic gravity anomaly, which has been modelled as a change in crustal thickness of the order of 10 km (Stern *et al.* 1987). Such a step in the Moho is approximately compatible with the increase in delay time seen at RAE.

Along with delay time there is also an increase in sediment depth from north to south (Figs 2 and 4). Typically *Vp*/*Vs* ratios for sediments are higher than those for crystalline basement. For orogenic belts such as those in New Zealand a representative *Vp*/*Vs* ratio for the crust of 1.73 is adopted (Christensen & Mooney 1995) and for Wanganui basin sediments *Vp*/*Vs* is >1.8 (Eberhart-Phillips *et al.* 2008). For these Vp/V_s ratios an increase in sediment thickness will result in an increase in delay time. To account for changes in sediment thickness a delay time correction is calculated using the sediment thickness below the station. The expected delay time is calculated for the sediment layer using a *Vp* of 3.4 km s^{-1} (Watson & Allen 1964) and Vp/V_s of 1.85. The difference between this delay time and the delay time calculated using the average crustal velocity of the NZST velocity model for the same H_s value gives a time correction for each station. This calculation of station corrections is relatively insensitive to the *Vp* values used, but sensitive to the *Vp*/*Vs* ratios. Sediment corrections vary from 0 for stations with no sediment to 0.37 s where the sediments are thickest.

Elevation also varies between stations, ranging from 700 m to near sea level. Elevation corrections are small (<0.1 s) in comparison to sediment corrections. Fig. 4 shows profiles of elevation, sediment depth and Moho delay times along the line from stations WRR in the south to MILC in the north. Even after taking into account the variation in delay times caused by elevation and sediment thickness there is still a 0.8 s increase in delay time for the Moho arrival between stations ERU and RAE. This is equivalent to ∼7 km increase in crustal thickness assuming *Vp*/*Vs* of 1.72 in the crust below the sediment layer.

At station KAI a strong Moho multiple is identified with arrival times between 10 and 12 s (Fig. 3a). Multiples can provide additional constraints on crustal thickness and geometry (Section 5.1.3).

4.1.2 Mantle conversions

In addition to the Moho arrivals, four stations (KAI, ERU, RAE and PAP) show a positive arrival at a delay time of ∼8 s (Fig. 3a). The delay time for this arrival decreases with increasing epicentral distance, which is indicative of a *Ps* conversion. An 8 s delay time puts the boundary at which this conversion occurs within the mantle at approximately 65 km depth, which still places it well above the subducted slab in this area (Ansell & Bannister 1996). Possible interpretations for this convertor will be discussed in Sections 5.1.4 and 6.3.

4.1.3 Crustal thickness

The *H*-*Vp*/*Vs* stacking method (Zhu & Kanamori 2000) has been used to stack receiver functions to determine crustal thickness (*H*) and *Vp*/*Vs* ratios. Because the $t_{PpSs+PsPs}$ phase is not observed in the receiver functions, only the *Ps* conversion and the *PpPs* multiple are stacked. Each phase is given equal weighting. The *H* range is restricted to 15–45 km (reasonable extremes for crustal thickness in the area) and *Vp*/*Vs* from 1.5 to 2.0. Initially *Vp* is set to an average crustal velocity of 6.0 km s^{-1} calculated from the New Zealand Standard model with the addition of a 1 km low-velocity (3.4 km s^{-1}) layer at the surface. Errors have been calculated by a boot-strap method that uses 200 randomly selected sample populations of receiver functions to determine the 95 per cent confidence interval.

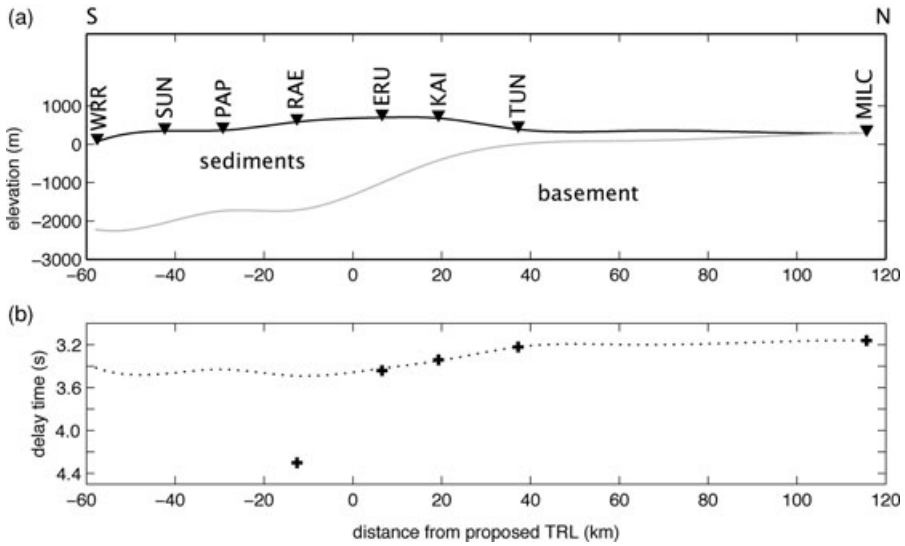

Figure 4. Expected delay time corrections due to sediments. A flat Moho is assumed. (a) A profile through stations WRR to MILC showing the station elevation (solid black line) and the sediment depth (solid grey line). Stations along the profile are shown as inverted triangles. (b) Delay times for Moho arrivals (crosses). Expected variation in Moho delay times given the sediment depth and elevation from (a) for a flat Moho are shown as a dotted line. Note that delay times for station WRR, SUN and PAP are not shown since no clear Moho arrival could be seen in the receiver functions for these individual stations.

This method of stacking is only appropriate where there is little lateral variability in *H* or *Vp*/*Vs*. Where this is not the case, phases will not stack coherently. Therefore this method has not been used where the path of the *PpPs* multiple crosses the proposed TRL. Because most of the events used in this study come from the north, use of this method is restricted to stations north of the proposed TRL. Lateral variation in sediment thickness will only have a small impact on the *Vp*/*Vs* ratio (1 km increase in sediment thickness approximately translates to a 0.01 increase in *Vp*/*Vs* ratio). Of the stations north of the proposed TRL, multiples can be clearly identified at station KAI (Fig. 3a) making it ideal for *H*-*Vp*/*Vs* stacking. Fig. 5(a) shows the stacking results for station KAI.

Two lines of positive stacking amplitude are observed. These are the contributions to the stack of the two phases; the steeper line corresponds to the *PpPs* multiple and the other corresponds to the *Ps* arrival. Where the two phases intersect, the stacking amplitude reaches a maximum. Stacking returns an *H* of 26.4 ± 1.5 km and a *Vp*/*Vs* of 1.72 ± 0.09.

For a region west of this study area (Sherburn & White 2005) derive a 1-D crustal velocity model from a local earthquake study that has much lower upper crustal velocities than the NZST (Maunder 2002). Controlled source data (Stratford & Stern 2006) also indicates that the average crustal *Vp* of the northwestern North Island is 5.8 km s^{-1}. Fig. 5(b) shows the stacking results using an average crustal *Vp* of 5.8 km s^{-1}. With this crustal *Vp*, stacking returns an *H* of 25.2 ± 1.5 km and *Vp*/*Vs* 1.74 ± 0.09. The stacking results using the two different crustal *Vp* values have overlapping uncertainties and are both in good agreement with the crustal thicknesses of 26 ± 2 km derived from a controlled source line to the north (Stratford & Stern 2006).

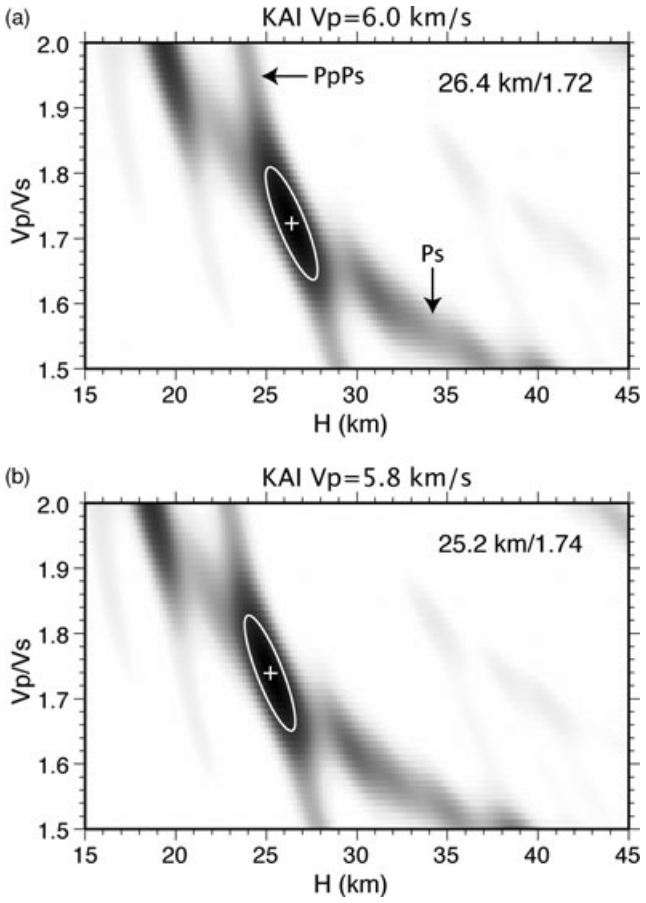

Figure 5. *H*-*Vp*/*Vs* stack results for station KAI. (a) shows results using a crustal *Vp* of 6.0 km s^{-1}. The contributions from the *Ps* and *PpPs* phases are labelled. (b) shows results using a crustal *Vp* of 5.8 km s^{-1}. Darker shades indicates higher stacking amplitude. The white cross indicates the peak amplitude and the white ellipse encompasses the 95 per cent confidence region. For *Vp* = 6.0 km s^{-1} the peak amplitude occurs at *H* = 26.4 km, *Vp*/*Vs* = 1.72. For *Vp* = 5.8 km s^{-1}, *H* = 25.2 km, *Vp*/*Vs* = 1.74.

Although the remaining TRAP stations north of the TRL do not have clear multiple arrivals, the information from station KAI can be used to estimate a crustal thickness. *Ps* arrivals from stations MILC, TUN, KAI and ERU range between 3.16 and 3.44 s. Without taking into account elevation or sediment thickness, this gives a depth range 23.6–25.9 km (using *Vp*/*Vs* 1.74) or 24.9–27.4 (using *Vp*/*Vs* 1.72).

From station ERU northward a crustal thickness of 25 ± 1.5 km is observed. If the same *Vp*/*Vs* ratios are applied to station RAE, a crustal thickness of 32 km is returned. This suggests there is a 7 km increase in crustal thickness between stations ERU and RAE.

4.1.4 CCP gathers and depth migration

H-*Vp*/*Vs* stacking provides an average crustal thickness and *Vp*/*Vs* ratio, over an area with a radius of up to 65 km, under the assumption that the structure sampled by P_ms and PpP_ms is 1-D. To study the lateral variations in subsurface features, common conversion point (CCP) stacking is used. This is a technique similar to common mid-point stacking used in seismic reflection studies, but predicted conversion points are used instead of source receiver midpoints. This method also has the advantage that coherent noise in the receiver functions from a single station, such as sediment reverberation, often becomes incoherent in multiple stations stacks (Dueker & Sheehan 1998).

The geographical stacking method of (Dueker & Sheehan 1997, 1998) has been used to make CCP gathers for stations in the TRAP array. For this stack we have only used receiver functions from events with epicentral distances $\geq 30^\circ$, however the results are almost indistinguishable from those done with the full set of receiver functions. Receiver functions are first bandpass filtered using a zero-phase second order Butterworth filter with corner frequencies of 0.2 and 1.5 Hz. This helps reduce the amplitude of long period sediment reverberations. A station correction for sediment depth and station elevation is then applied. These are the only lateral variation corrections made for this data since tomographic modelling indicates there is little variation in crustal *Vp*/*Vs* ratios below 4 km along the TRAP array (Reyners *et al.* 2006). P_ds (*P*-to-*S* conversion at depth *d*) piercing points are found by ray tracing the converted *S*-wave ray paths using a 1-D velocity model and Snell's law. Piercing points are geographically binned using a 2-D vertical grid of sample points. Receiver functions are mapped along their ray paths traced in three dimensions through a flat-layered velocity model, which corrects for event-station moveout while at the same time performing a pre-stack depth migration. This step is performed using the same flat-layered velocity model used for ray tracing. All rays within a bin are summed to form a stacked trace for each horizontal bin, creating a 2-D depth section.

The NZST velocity model (Maunder 2002) is used as an initial 1-D velocity model to give both *P* and *S*-wave velocities. The crustal *Vp*/*Vs* ratio of this model is 1.71 down to 25 km, which is slightly lower than estimates from *H*-*Vp*/*Vs* stacking, but within the uncertainties. Since receiver functions in the CCP stacks are already

corrected for the high *Vp*/*Vs* sediments, the *Vp*/*Vs* ratio should be lower than the values indicated by *H*-*Vp*/*Vs* stacking (where sediment corrections are not applied) by up to 0.03 so the model *Vp*/*Vs* ratio is acceptable. The only significant difference between this model and active source data (Stratford & Stern 2006) to 25 km deep, is that the top 2 km of low velocity material, which has already been compensated for in the station corrections for sediment depth. For a Moho up to 25 km depth these two models are therefore nearly indistinguishable and for a deeper Moho the NZST velocity model is more appropriate.

Since the primary focus is the topography of the Moho, horizontal bin width is set to the estimated width of the first Fresnel zone for an interface at 30 km depth. Assuming a signal frequency of 1.5 Hz and an *S*-wave velocity of 3.4 km s^{-1}, horizontal bin widths are set to 8 km. The vertical bin width is set to 1 km as this is less than the estimated of vertical resolution, which is approximated as 1/2 of the minimum wavelength (∼2 km).

The out of plane distance of ray paths has not been limited. For a north–south section through the array, the out of plane distance for a piercing point at 30 km depth is less than 20 km and for 70 km depth, piercing points are up to 30 km out of plane. For a boundary which dips out of plane the maximum dip, θ, which will stack into the 2-D depth section coherently for the entire out of plane width can be calculated using $\theta = \arctan(\lambda/2y)$, where y is the out of plane distance to the piercing point. For an *S*-wave velocity of 3.5 km s^{-1} and a signal frequency of 1.5 Hz this equates to a maximum dip of $<5^{\circ}$.

CCP gathers in the depth-distance domain as a south to north cross-section of the TRAP array are plotted (Fig. 6). The main focus here is on the Moho conversion labelled as P_ms and MOHO. In the north (distances > 0) this is a prominent horizontal positive feature at around 25 km depth. The Moho conversion remains reasonably horizontal even when no correction for lateral variation is applied. There is a step in Moho depth between stations RAE and ERU. In the south the Moho conversion is deeper (>30 km), weakens and dips southward reaching 35 km depth below station SUN. A thickened crust here is consistent with a deep seismic reflection profile 70 km to the southeast (Fig. 2), which shows a reflection Moho depth between 37 and 42 km (Stern & Holt 1994).

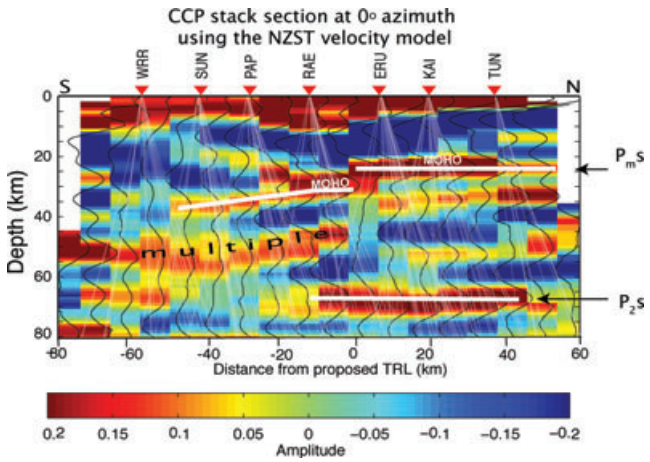

Figure 6. S/N CCP stack section for the TRAP array using the NZST. Red colours indicate positive phases, blue colours indicate negative phases, Gathers have been corrected for sediment depth and elevation. The Moho conversion is labelled P_ms. This conversion is nearly flat north of station RAE. There is a step in Moho depth between stations RAE and ERU. South of RAE the Moho conversion dips southward. The mantle conversion is labelled P_2s. Fine white lines show ray paths for converted phases to respective stations.

The dipping section of the Moho conversion is lower in amplitude than the northern section. Since most of the events used are up-dip of the stations, a drop in Moho amplitude for the dipping section is expected (e.g. Cassidy 1992). Moreover, synthetic modelling shows that as sediment thickness increases, multiples from the sediment layer will interfere and weaken the Moho conversion (Salmon 2008).

A strong positive phase is seen at a depth of ∼32 km, immediately below the *Ps* converter at the northern end of the line (Fig. 6). This phase can be further tracked across the stacked section to be at an apparent depth of ∼50 km beneath WRR. At station KAI this phase corresponds to the positive peak seen at ∼5 s (Fig. 3a) and its moveout suggests that it is a multiple from a mid-crustal boundary at 10–15 km depth.

A strong positive conversion with lateral coherence is apparent (Fig. 6) below the Moho at ∼65 km depth (labelled P_2s). P_2s is coherent between stations TUN and RAE but disappears south of station RAE. The positive phase on the receiver functions, indicates that the boundary represents a transition from low to higher seismic velocities. There are no multiples from this boundary with which to constrain the *Vp*/*Vs* ratio and depth, however the error in depth can be estimated by using the NZST velocity model down to 25 km depth and varying the *Vp*/*Vs* ratio for the mantle between 1.7 and 1.8 and the mantle velocity between 7.2 and 8.2 km s^{-1}. Within these bounds the depth to the P_2s boundary is 65 ± 5 km and approximately coincides with an increase in *Vp*/*Vs* ratio seen in tomographic images (Reyners *et al.* 2006) and with an increase in seismic attenuation. This conversion is above the expected projection of the subducted slab (Ansell & Bannister 1996) but appears to be truncated close to the in plane projection of the slab (see Section 5). A similar mantle boundary is observed at 75–100 km depth in the mantle wedge below Tonga and has been associated with compositional zonation caused by fluids rising through the wedge (Zheng *et al.* 2007). Without more data and a wider mapping of this feature, its interpretation remains uncertain.

An alternative summary presentation of the TRAP data shows receiver functions for all the stations north and south of the TRL stacked in ray parameter (p) bins (Fig. 7). Bin widths are 0.09 s km^{-1} wide and are spaced at 0.03 s km^{-1} centres. Receiver functions have been corrected for sediment thickness and elevation prior to stacking. For the northern stations (Fig. 7a) a prominent positive phase can be seen at ∼3.1 s, which corresponds to a NZST velocity model depth of 25 km. The mantle phase seen on the CCP stacks is less obvious in this plot but can be seen as a positive phase between 7 and 8 s. The Moho multiple arrives slightly after the moveout curve predicted by the model, most likely due to the effect of surface sediments on the first two crustal legs of travel, which have not been corrected for. A positive phase can also be seen ∼1 s after the Moho arrival. This phase corresponds to the positive phase paralleling the Moho arrival in the stacked section (Fig. 6). Delay times for this phase decrease with increasing ray parameter, supporting the view that this phase is a mid-crustal multiple.

For the stations south of the TRL (Fig. 7b) the stacking shows a clear positive phase at 4–5 s. This phase corresponds to a Moho depth of 35 km south of the TRL. Thus on average there is a 10 km change in crustal thickness across the TRL, but in detail (Fig. 6) there is a 7 km step followed by a southward dipping ramp along which the Moho deepens by another 3 km. A southward dip in the Moho at the southern end of this study is also inferred from gravity

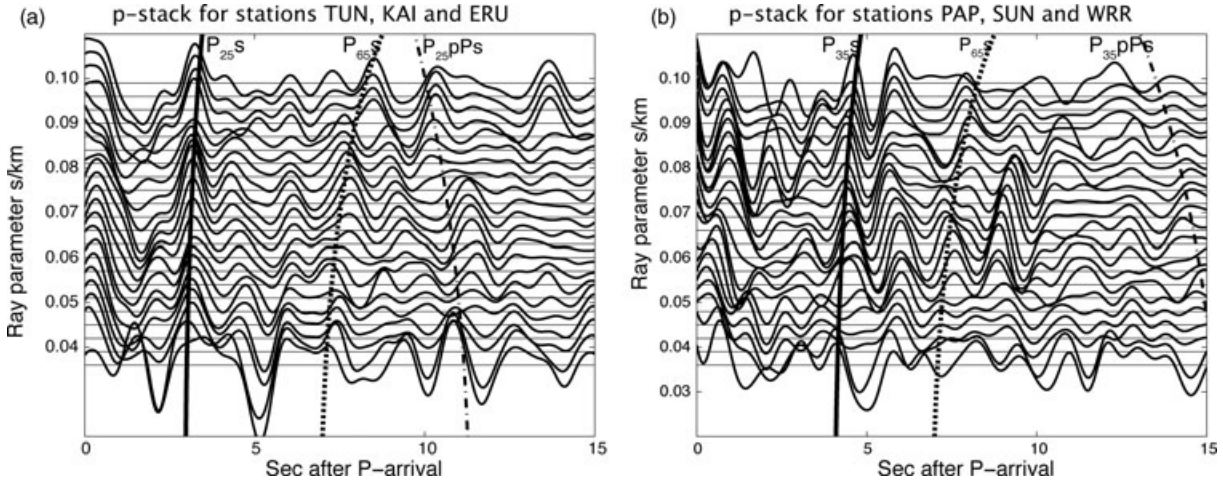

Figure 7. Ray parameter stacks for station groups. (a) Stations north of the TRL. *Ps* phase moveout curves are shown for the NZST model for 25 km (solid line labelled $P_{25}s$) and 65 km (dotted line labelled $P_{65}s$). The *PpPs* phase moveout curve is also shown (dashed line labelled $P_{25}pPs$). (b) Stations south of the TRL. *Ps* phase moveout curve are shown for the NZST model for 35 km (solid line labelled $P_{35}s$) and 65 km (dotted line labelled $P_{65}s$). The *PpPs* phase moveout curve is also shown (dashed line labelled $P_{35}pPs$)

modelling (Ewig 2009) and an offshore seismic line (Holt & Stern 1994; Fig. 2).

4.2 Dipping layers

Receiver function analysis in the previous sections uses the assumption of flat-layered isotropic velocity models. Despite this, results of CCP stacking clearly indicate the presence of a step in the Moho between stations ERU and RAE along with a southward dipping Moho south of station RAE (Fig. 6). Dipping layers will introduce an azimuthal dependence to receiver functions (Jones & Phinney 1998; Savage 1998). For a southward dipping crust–mantle boundary the amplitude of a Moho conversion will be reduced for events from the north and increased for events from the south. This would help to explain the absence of an obvious Moho conversion in receiver functions for individual stations south of RAE.

4.1.5 Magnetotelluric image of the TR-line

A magnetotelluric study was conducted across the TRL in parallel with the seismic study. Stations for the MT consisted of a Phoenix^{TM} system located close to each seismic station (Fig. 1). Further details of this survey can be found in Salmon (2008). Data were recorded at sites for up to 64 hr. Data were modelled using a finite element inversion scheme (Wannamaker *et al.* 1987).

Low resistivities ($<$100 Ohm-m) are evident at depths of about 23 km north of the TRL line. Such a resistivity in dry peridotite would require temperatures $>$1300 °C (Wang *et al.* 2006; Salmon 2008). The presence of water in the nominally anhydrous mantle minerals, however, would allow the same resistivity but with temperatures of 900 $\pm$ 50 °C (Wang *et al.* 2006). South of the TR-line resistivities reach 1000 Ohm-m at depths greater than 15 km (Fig. 8) and this is a typical value for the crust and a colder upper mantle (Schilling *et al.* 1997). Using the relationship of Wang *et al*. (2006) between conductivity, temperature and water content, a temperature of about 650 °C is predicted in the upper mantle south of the TR-line (Fig. 8).

Sediment thickness variations are well represented by low resistivities ($\sim$10 Ohm-m) in the MT profile as the mudstone sediments that dominate this area are water saturated and thus will be highly conductive. We note an apparent correlation of a local thinning of sediment at MT station 005 (Fig. 8) with a similar local narrowing in the first positive phase of the receiver function stack beneath station SUN (Fig. 6). This is in keeping with both theory and observations that show sediments broadening the first peak of receiver functions (Ammon *et al.* 1990).

5 DISCUSSION: TECTONIC SIGNIFICANCE

There are four geophysical properties that underscore both the sharpness and the fundamental character of the subsurface expression of the TR-line; Moho offset from receiver functions; steep regional gravity gradient (Fig. 1); electrical resistivity (Fig. 8) and sharp change in seismic attenuation of *P* waves (Salmon *et al.* 2005; Eberhart-Phillips *et al.* 2008). A strong change in anisotropy (Audoine *et al.* 2004; Greve *et al.* 2008) occurs in the vicinity of the TR line, but there are insufficient data to describe the 2-D character of this change. These data combine to show that the TR-line is the surface expression of a boundary across which the crust thins and the mantle lithosphere either thins dramatically or vanishes. If there are such sharp variations in the thickness of the crust and the mantle lid, then large deviatoric stresses, and hence earthquakes, should be present.

5.1 Seismicity

Seismicity linked to the TR-line is well known (Hatherton 1970b; Reyners 1980b) and clear in both cross-section and plan view (Figs 9a–c). Hypocentres span the depth range of 20–40 km on or adjacent to the line (Figs 9b and c) and uncertainties on vertical locations of New Zealand earthquakes, shallower than 40 km, are typically of the order of $\pm$2 km. (Hatherton 1970a; Reyners 1980a, 2010; Sherburn & White 2005). In particular, there is a close spatial relationship between the Moho offset and the cluster of seismicity as noted previously (Stern *et al.* 2006). Sherburn & White (2005) argue that the Moho offset is 20 km north of the TR-line, allowing all the seismicity to be in the thicker lower crust to the south of

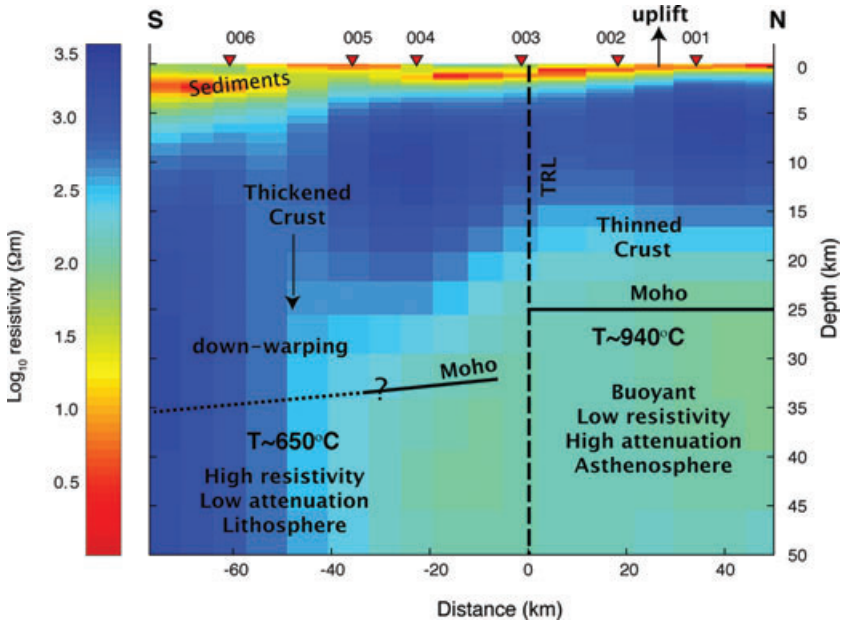

Figure 8. Interpretation of the 2-D electrical resistivity model across the TR-line. The Moho interpretation is from the receiver function analysis (Fig. 6) with the question mark signifying that we cannot distinguish between a vertical step or one dipping at an angle as low as 45°. The region north of the TR-line has thinned crust. Resitivities of <100 Ohm-m at depths >25 km are interpreted as a hot and wet upper mantle with a temperature of ∼950 °C (see text). Low resistivities (<25 Ohm-m) in the top 5 km show the extent of the sediments along the profile.

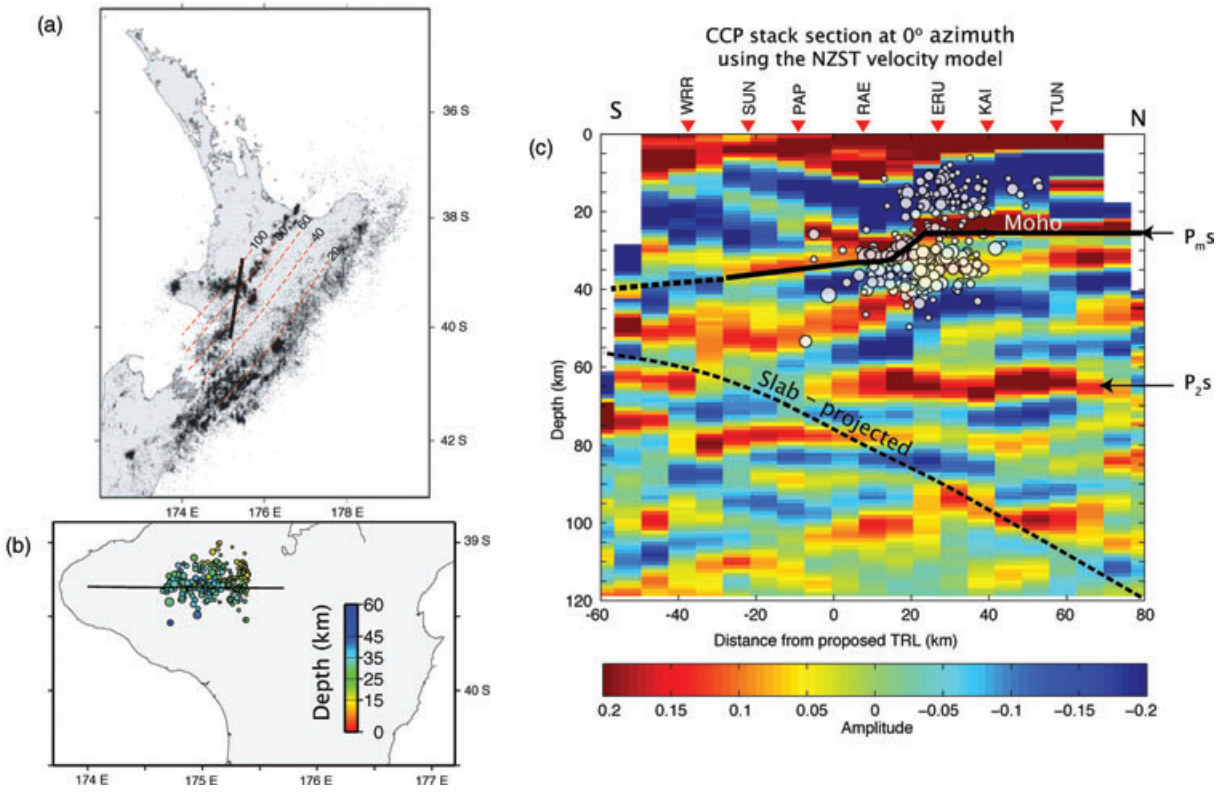

Figure 9. (a) Map of crustal (<33 km) seismicity for North Island during period 1990–2007 magnitude ranges 0.3–6.99 from Geonet web site (http://geonet.org.nz). Note distinctive band of seismicity striking east west at almost right angles to strike plate boundary. Red contours indicate depth to the subducting slab (Ansell & Bannister 1996). (b) Location and depths of earthquakes along TR-line that are displayed on (c). Uncertainty in depths is at most ±2 km. Magnitudes range from 0.9 to 4.0. (c) CCP stack (as of Fig. 6) with earthquake hypocenters superimposed. We also show as the curved dashed line the projection of the subducted Pacific Plate beneath the profile. Note that the strike of the Pacific Plate is about 45° whereas that of the profile is about 010°.

the TR-line. The results of this study, however, clearly show the Moho-offset sits directly beneath the TR-line and is coincident with the strongest gravity gradient. Our interpretation of the TR-line at depth requires, therefore, some of the seismicity to be in the mantle and some in the crust.

5.2 Causes of the step

The key question is what is the collective cause of all phenomena seen at or beneath the TR-line? Both Moho offsets of 7 km and deep seismicity (20–40 km) in both the crust and upper mantle are unusual in the continents (Jackson *et al.* 2008). One published interpretation of seismicity associated with the TR-line is that it represents the flow of fluids into an area that weakens faults to the point of strain release (Reyners *et al.* 2007). This interpretation has three difficulties. First there are no known east–west faults anywhere in the western North Island (NZGS Map 1972). Second, why are the earthquakes in the lower crust/upper mantle and not upper crust? Finally, this interpretation does not explain the clear association of a Moho offset with the earthquakes. While water may have some part to play in triggering earthquakes, it is not clear how fluids can cause 7 km offsets in the Moho. Reyners *et al*. also interpreted the change in anisotropy (Audoine *et al.* 2004) to be caused by change in fluid flow across the boundary, but another interpretation is that thick lithosphere in the south has a strong signal from previous strike-slip deformation, while such lithosphere is absent to the north. An alternative reason why we observe such deep seismicity in this area of instability and strong deviatoric stress is that the strain rates are sufficiently high that even at 900 °C, earthquakes can occur (Keir *et al.* 2009). However, we see both high strain rates and fluids as effects, not causes, of the phenomena described herein.

We propose a causal link between the unusually deep earthquakes, the Moho offset, the flat and shallow Moho of western North Island, and the geophysical evidence, described above and summarised in Stern *et al*. (2006), of missing mantle lid north of the TR-line. Mechanisms that can remove the mantle lid have been discussed elsewhere and can be listed as: mantle delamination (Bird 1979), intracontinental subduction (Mattauer 1996) or convective removal of over thickened mantle lithosphere (Neil & Houseman 1999). We argue for one or a combination of these three mechanisms.

Seven key observations from central and western North Island have been presented as evidence for a late Miocene convective removal of mantle lithosphere (Stern *et al.* 2006).

1. Rapid (<5 Myr) and regional (wavelength ∼300 km) uplift of western North Island in the Pliocene.
2. Rapid Pliocene subsidence of southwestern North Island at a depocentre that is about 100 km south of the region of uplift.
3. A zone between the uplift and subsidence zones along which there is a near vertical offset of both the Moho, and offset in mantle lid thickness and localized seismicity to depths of 45 km beneath the offset (this study).
4. Pliocene, high-K volcanism in the region of uplift.
5. A sequence of sedimentary basin depocentres whose ages show an apparent migration with time from north to south.
6. Seismological (Horspool *et al.* 2006) and buoyancy analysis (Pulford & Stern 2004) evidence to show that north of the Taranaki-Ruapehu line there is little if any mantle lithosphere as far north as Auckland City.
7. Shear wave splitting showing the only place in New Zealand with consistent nulls, being in the region north of the TR line (Greve *et al.* 2008)—this observation is consistent with missing mantle lithosphere here if the predominant mode of creating SKS splitting is shearing the mantle lid (Molnar *et al.* 1999).

These observations link the Oligocene–Miocene history of shortening in the western North Island to the driver of thickened mantle, and thus the proposed loss of a Rayleigh Taylor–type of instability. However, other mantle lid removal mechanisms cannot be ruled out. For example, we note the similarity of our receiver function profile (Fig. 6) with that derived from the Sierra Nevada of the western USA where a mantle instability is ascribed to the removal of thickened, high density lower crust (Frassetto *et al.* 2010).

6 CONCLUSIONS

1. Receiver functions define a Moho offset of 7–10 km across the Taranaki-Ruapehu line in North Island, New Zealand.
2. To the north of the TR-line a Moho depth of 25 ± 1.5 km is defined, which is consistent with other seismic measurements of Moho depth in this region.
3. Electrical resistivity, gravity, seismic anisotropy and seismic attenuation all help to define a sharp boundary in the upper mantle as well as the crust beneath the TR-line.
4. Anomalously deep crust and upper mantle seismicity is associated with the TR-line suggesting strong deviatoric stresses and /or high strain rates.
5. The most likely cause of all phenomena seen at the TR-line is some form of convective removal of the mantle lid and lower crust to the north of the TR-line.

ACKNOWLEDGMENTS

We thank FRST, GeoNet, Hugh Bibby and GNS Science funding, for data, advice and equipment, A GNS PhD scholarship supported M. Salmon for much of the field work. Wanda Stratford and Graham Stuart provided constructive criticism of earlier drafts of this paper.

REFERENCES

Adams, R. & Ware D., 1977. Subcrustal earthquakes beneath New Zealand: locations determined with a laterally inhomogeneous velocity model, *N. Z. J. Geol. Geophys.,* **20,** 59–83.

Ammon, C.J., Randell G.E. & Zandt G., 1990. On the non-uniqueness of receiver function inversions, *J. geophys. Res.,* **95,** 15 303–15 318.

Anderton, P.W., 1981. Structure and evolution of the South Wanganui Basin, *N.Z. J. Geol. Geophys,* **24,** 39–63.

Ansell, J. & Bannister S., 1996. Shallow morphology of the subducted Pacific plate along the Hikurangi margin, New Zealand, Phys. *Earth planet. Inter.*, **93,** 3–20.

Audoine, E., Savage M.K. & Gledhill K., 2004. Anisotopic structure under a back-arc spreading region, the Taupo Volcanic Zone, New Zealand, *J. geophys. Res,* **109,** B11305, doi:10.1029/2003JB002932.

Bannister, S., Reyners M., Stuart G. & Savage M., 2007. Imaging the Hikurangi subduction zone, New Zealand, using teleseismic receiver functions; crustal fluids above the forearc mantle wedge, *Geophys. J. Int.,* **169,** 602–616.

Bird, P., 1979. Continental delamination and the Colorado Plateau, *J. geophys. Res.,* **84,** 7561–7571.

Cassidy, J.F., 1992. Numerical experiments in broadband receiver function analysis, *Bull. seism. Soc. Am.,* **82,** 1453–1474.

Christensen, N.I. & Mooney W.D., 1995. Seismic velocity structure and composition of the continental crust: a global review., *J. geophys. Res.,* **100,** 9761–9788.

Dickinson, W.R., 2003. The Basin and Range Province as a composite extensional domain, in *The George A. Thompson Volume: the Lithosphere of Western North America and its Geophysical Characterization,* eds Klemperer, S.L. and Ernst S.L., Geological Society of America, Boulder, CO.

Doll, W.E., Domoracki W.J., Costain J.K., Çoruh C., Ludman A. & Hopeck J.T., 1996. Seismic reflection evidence for the evolution of a transcurrent fault system: the Norumbega fault zone, Maine., *Geology,* **24,** 251–254.

Dueker, K.G. & Sheehan A.F., 1997. Mantle discontinuity structure from midpoint stacks of converted P to S waves across the Yellowstone hotspot track, *J. geophys. Res.,* **102,** 8318–8327.

Dueker, K.G. & Sheehan A.F., 1998. Mantle discontiniuity structure beneath the Colorado Rocky Mountains and High Plains, *J. geophys. Res.,* **103,** 7153–7169.

Eberhart-Phillips, D., Reyners M., Chadwick M. & Stuart G., 2008. Three-dimensional attenuation structure of the Hikurangi subduction zone in the central North Island, New Zealand, *Geophys. J. Int.,* **174,** 418–434.

Ewig, E., 2009. Lithospheric shortening and ductile deformation in a back-arc setting: South Wanganui Basin, New Zealand, *PhD thesis*, Victoria University of Wellington, Wellington.

Frassetto, A., Zandt, G., Gilbert, H., Owens, T. & Jones, C., 2010. Improved imaging with phase-weighted common conversion point stacks of receiver functions, *Geophys. J. Int.,* **182,** 368–374, doi:10.1111/j.1365-246X.2010.04617.x.

Gerrard, M., 1971. Tupapakurua-1, *Petroleum Report Series*, ANZPAC Petroleum Corp.

Greve, S.M., Savage M.K. & Hofman S.D., 2008. Strong variations in seismic anisotropy across the Hikurangi subduction zone, North Island, New Zealand, *Tectonophysics,* **462,** 7–21.

Gurrola, H., Minster J.B. & Owens T.J., 1994. The use of velocity spectrum for stacking receiver functions and imaging upper mantle discontinuities, *Geophys. J. Int.,* **117,** 427–440.

Hatherton, T., 1969. The geophysical significance of calc-alkaline andesites in New Zealand., *N. Z. Geol. Geophys.,* **12,** 436–459.

Hatherton, T., 1970a. Upper mantle inhomogenity beneath New Zealand: surface manifestations, *J. geophys. Res.,* **75,** 269–284.

Hatherton, T., 1970b. Upper mantle inhomogenity beneath New Zealand: surface manifestations., *J. geophys. Res.,* **75,** 269–284.

Hayward, B. *et al*., 2001. K-Ar ages of early Miocene arc-type volcanoes in northern New Zealand, *N.Z. J. Geol. Geophys.,* **44,** 285–311.

Holt, W.E. & Stern T.A., 1994. Subduction, platform subsidence & foreland thrust loading: the late Tertiary development of Taranaki Basin, New Zealand, *Tectonics,* **13,** 1068–1092.

Horspool, N., Savage M.K. & Bannister S., 2006. Implications for intraplate volcanism and back-arc deformation in northwestern New Zealand, from joint inversion of receiver functions and surface waves, *J. geophys. Res.,* **166,** 1466–1483.

Jackson, J., McKenzie D., Preistley K. & Emmerson B., 2008. New views on the structure and rheology of the lithosphere, *J. Geol. Soc. Lond.,* **165,** 453–465.

Jones, C. & Phinney R.A., 1998. Seismic structure of the lithosphere from teleseismic converted arrivals observed at small arrays in the southern Sierra Nevada and vicinity, California, *J. geophys. Res.,* **103,** 10 065–10 090.

Keir, D., Bastow I.D., Whaler K.A., Daly E., Cornwell D.G. & Hautot S., 2009. Lower crustal earthquakes near the Ethiopian rift induced by magmatic processes, *Geochem., Geophys., Geosyst.,* **10,** Q0AB02, doi:10.1029/2009GC002382.

Kennett, B.L.N., Engdahl E.R. & B.R., 1995. Constraints on seismic velocities in the Earth from travel times, *Geophys. J. Int.,* **122,** 108–124.

Langston, C.A., 1979. Structure under Mount Rainier, Washington, inferred from teleseismic body waves, *J. geophys. Res.,* **84,** 4749–4762.

Mattauer, M., 1996. Intracontinental subduction, crust-mantle decollement and crustal stacking wedge in the Himalayas and other collision belts, in *Collision Tectonics,* Vol. 19, pp. 37–50, eds Coward, M.P. and Ries, A.C., Geol Soc. of London Spec. Pub.

Maunder, D.E., 2002. *New Zealand Seismological Report 2000*, Seismological Observatory Bulletin E-183, Institute of Geological and Nuclear Sciences.

McBride, J.H., 1994. Structure of a continental strike-slip fault from deep seismic reflection: Walls Boundary fault, northern British Caledonides., *J. geophys. Res.,* **99,** 23 985–24 005.

Molnar, P., *et al*. 1999. Continuous deformation versus faulting through the continental lithosphere of New Zealand, *Science,* **286,** 516–619.

Mooney, H.M., 1970. Upper mantle inhomogeneity beneath New Zealand: seismic evidence., *J. geophys. Res.,* **75,** 285–309.

Neil, E.A. & Houseman G.A., 1999. Rayleigh-Taylor instability of the upper mantle and its role in intraplate orogeny, *Geophys. J. Int.,* **138,** 89–107.

New Zealand Geological Survey, 1972. *North Island (1st edn) Geological Map of New Zealand 1:1 000 000*, Dept. Sci. Indus. Res., Wellington.

Owens, T.J. & Zandt G., 1985. The response of the continental crust-mantle boundary observed on broadband teleseimic receiver functions, *Geophys. Res. Lett.,* **12,** 705–708.

Park, J. & Levin V., 2000. Receiver functions from multi-taper spectral correlation estimates, *Bull. seism. Soc. Am.,* **90,** 1507–1520.

Price, R.C., Stewart R.B., Woodhead J.D. & Smith I.E. M., 1999. Petrogenesis of high-K arc magmas: evidence from Egmont Volcano, North Island, New Zealand, *J Petrol.,* **40,** 167–197.

Pulford, A. & Stern T.A., 2004. Pliocene exhumation and landscape evolution of central North Island, New Zealand: the role of the upper mantle, *J. geophys. Res.,* **109,** doi:10.1029/2003jf000046.

Reyners, M., 1980. A microearthquake study of the plate boundary, North Island, New Zealand, *Geosphys. J. R. astr. Soc.,* **63,** 1–22.

Reyners, M., 2010. Stress and strain from earthquakes at the southern termination of the Taupo Volcanic Zone, New Zealand, *J. Volc. Geotherm. Res.,* **190,** 82–88.

Reyners, M., Eberhart-Phillips D., Stuart G. & Nishimura Y., 2006. Imaging subduction from the trench to 300 km depth beneath the central North Island, New Zealand, with Vp and Vp/Vs, *Geophys. J. Int.,* **165,** 565–583.

Reyners, M., Eberhart-Phillips D. & Stuart G., 2007. The role of fluids in lower-crustal earthquakes near continental rifts, *Nature,* **446,** 1075.

Salmon, M., Savage M.K. & Stern T.A., 2005. Seismic attenuation, temperature, H20, mantle melting and rock uplift, Central North Island New Zealand, *EOS, Trans. Am. geophys. Un.,* **86,** 52, Fall Meet. Suppl., Abstract T13B-0478.

Salmon, M.L., 2008. Crust and upper mantle inhomgenities beneath western North Island, New Zealand: evidence from seismological and electromagnetic data, *PhD thesis*, Victoria University of Wellington, Wellington.

Savage, M.K., 1998. Lower Crustal anisotropy or dipping layers? Effects on receiver functions and a case study in New Zealand, *J. geophys. Res.,* **103,** 15 069–15 089.

Schilling, F., Partzsch G., Brasse H. & Schwarz G., 1997. Partial melting below the magmatic arc in the central Andes deducd from electromagnetic field experiements, *Phys. Earth planet. Inter.,* **103,** 17–31.

Seward, A., Hendreson C. & Smith E., 2009. Models of the upper mantle beneath the central North Island, New Zealand, from speeds and anisotropy of subhorizontal P waves Pn, *J. geophys. Res.,* **114,** B01301, doi:10.1029/2008JB005805.

Seward, A.M., Henderson,C.M. & Smith E.G.C., 2008. Models of upper mantle beneath the Central North Island, New Zealand, from speeds and anisotropy of sub-horizontal P-waves Pn, *J. geophys. Res.,* **114,** B01301, doi:10.1029/2008JB005805.

Shearer, P.M., 1999. *Introduction to Seismology,* Cambridge University Press, Cambridge, 257 pp.

Sherburn, S. & White R., 2005. Crustal seismicity in Taranaki, New Zealand using accurate hypocentres from a dense network, *Geophys. J. Int.,* **162,** 494–506.

Sheriff, R.E. & Geldart L.P., 1995. *Exploration Seismology,* 2nd edn, Cambridge University Press, Cambridge.

St John, D., 1964. *Parikino-1 Exploration Well Resume*, Petroleum Report Series, Shell BP and Todd Oil Services Ltd.

Stern, T.A. & Holt W.E., 1994. Platform subsidence behind an active subduction Zone., *Nature,* **368,** 233–236.

Stern, T.A., Smith E.G.C., Davey F.J. & Muirhead K.J., 1987. Crustal and upper mantle structure of northwestern North Island, New Zealand, from seismic refraction data, *Geophys. J. R. astr. Soc.,* **91,** 913–936.

Stern, T.A., Stratford W.R. & Salmon M.L., 2006. Subduction at a continental margin: kinematics and dynamics of the central North Island, New Zealand, *Rev. Geophys.,* **44,** RG4002, doi:10.1029/2005RG000171.

Stratford, W. & Stern T., 2006. Crust and upper mantle structure of the continental backarc:central North Island, New Zealand, *Geophys. J. Int.,* **166,** 469–484.

Vinnik, L., 1977. Detection of waves converted from P to SV in the mantle, *Phys. Earth planet. Inter.,* **15,** 39–45.

Wang, D., Mookherjee Y., Xu Y. & Karato S., 2006. The effect of water on electrical conductivity of olivine, *Nature,* **443,** 977–980.

Wannamaker, P.E., Stodt J.E. & Rijo L., 1987. A stable finite element solution for two dimensional magnetotelluric modelling, *Geophys. J. Int.,* **88,** 277–296.

Watson, J. & Allen D., 1964. *Compilation of Seismic Results in Wanganui Basin*, Petroleum Report Series, Shell BP and Todd Oil Services Ltd.

Wilson, C.K., Jones C.H., Molnar P., Sheehan A.F. & Boyd O.S., 2004. Distributed deofrmation in the lower crust and mantle beneath a continental strike slip fault zone: Marlborough fault system, South Island, New Zealand, *Geology,* **32,** 837–840.

Zheng, Y., Lay T., Flanagan M. & Williams Q., 2007. Pervasive seismic wave reflectivity and metasomatism of the Tonga mantle wedge, *Science,* **316,** 855–859.

Zhu, L. & Kanamori H., 2000. Moho depth variation in southern California from teleseismic receiver functions, *J. geophys. Res.,* **105,** 2669–2980.